ORIGINAL ARTICLE

The translocator protein ligand [18F]DPA-714 images glioma and activated microglia in vivo

Alexandra Winkeler · Raphael Boisgard · Ali R. Awde · Albertine Dubois · Benoit Thézé · Jinzi Zheng · Luisa Ciobanu · Frédéric Dollé · Thomas Viel · Andreas H. Jacobs · Bertrand Tavitian

Abstract

Purpose In recent years there has been an increase in the development of radioligands targeting the 18-kDa translocator protein (TSPO). TSPO expression is well documented in activated microglia and serves as a biomarker for imaging neuroinflammation. In addition, TSPO has also been reported to be overexpressed in a number of cancer cell lines and human tumours including glioma. Here we investigated the use of [18F]DPA-714, a new TSPO positron emission tomography (PET) radioligand to image glioma in vivo.
Methods We studied the uptake of [18F]DPA-714 in three different rat strains implanted with 9L rat glioma cells: Fischer (F), Wistar (W) and Sprague Dawley (SD) rats. Dynamic [18F]DPA-714 PET imaging, kinetic modelling of PET data and in vivo displacement studies using unlabelled DPA-714 and PK11195 were performed. Validation of TSPO expression in 9L glioma cell lines and intracranial 9L gliomas were investigated using Western blotting and immunohistochemistry of brain tissue sections.
Results All rats showed significant [18F]DPA-714 PET accumulation at the site of 9L tumour implantation compared to the contralateral brain hemisphere with a difference in uptake among the three strains (F>W>SD). The radiotracer showed high specificity for TSPO as demonstrated by the significant reduction of [18F]DPA-714 binding in the tumour after administration of unlabelled DPA-714 or PK11195. TSPO expression was confirmed by Western blotting in 9L cells in vitro and by immunohistochemistry ex vivo.
Conclusion The TSPO radioligand [18F]DPA-714 can be used for PET imaging of intracranial 9L glioma in different rat strains. This preclinical study demonstrates the feasibility of employing [18F]DPA-714 as an alternative radiotracer to image human glioma.

Keywords Glioma · Translocator protein · TSPO · Microglia · Positron emission tomography · Peripheral benzodiazepine receptor · [18F]DPA-714

A. Winkeler · R. Boisgard · A. R. Awde · A. Dubois · B. Thézé ·
J. Zheng · B. Tavitian (✉)
Inserm, U1023, Laboratoire d'Imagerie Moléculaire
Expérimentale, Université Paris Sud,
Orsay, France
e-mail: bertrand.tavitian@cea.fr

L. Ciobanu
CEA, DSV, I2BM, NeuroSpin, LRMN,
Gif sur Yvette, France

T. Viel · A. H. Jacobs
European Institute for Molecular Imaging (EIMI),
Westfälische Wilhelm-Universität Münster (WWU),
Münster, Germany

A. Winkeler · R. Boisgard · A. R. Awde · A. Dubois · B. Thézé ·
J. Zheng · F. Dollé
CEA, I2BM, SHFJ,
4 place du Général Leclerc,
91400 Orsay, France

Introduction

The 18-kDa translocator protein (TSPO), also known as the peripheral benzodiazepine receptor, is a protein of the outer mitochondrial membrane expressed in peripheral organs and is particularly enriched in steroidogenic tissue. In the central nervous system (CNS) TSPO expression is low and limited to resident glial cells [1].

However, cerebral TSPO expression is dramatically increased after glial cell activation and has become a well-characterized marker for neuroinflammation [2–6]. In addition, TSPO levels are also elevated in a number of cancer cell lines and human tumours including breast, ovary, colon

and prostate cancer, as well as glioma [7, 8]. Initial studies on TSPO and TSPO ligands in the brain carried out in the 1980s and 1990s indicated that the density of TSPO was high in malignant gliomas [9–12] and in glioma cell lines [9–14]. Further studies demonstrated that TSPO expression levels positively correlated with the grade of malignancy and showed a negative correlation between TSPO expression and survival [15, 16]. In the late 1980s positron emission tomography (PET) imaging of human gliomas using TSPO radioligands was suggested [11–13] and first demonstrated with the isoquinoline derivative [11C]PK11195 [10, 17]. However, numerous limitations of this radioligand have been reported, including the high level of non-specific binding and the relatively poor signal-to-noise ratio [2].

In the last few years many efforts have been undertaken in the development of new radioligands targeting the TSPO. Thus, recently developed radioligands with improved in vivo specificity for TSPO may have the potential to improve PET imaging of TSPO expression in human gliomas. One of the promising new radioligands for TSPO imaging is the pyrazolo[1,5]pyrimidine [18F]DPA-714. [18F]DPA-714 demonstrated lower non-specific uptake and higher binding potential (BP) as compared to [11C]PK11195 in a rat model of acute neuroinflammation [18]. The aim of the present study was to investigate the potential use of [18F]DPA-714 as a new PET imaging marker for glioma. Here we report the use of [18F]DPA-714 to monitor TSPO-expressing gliomas in vivo using PET imaging. The specificity of the radioligand binding was confirmed by displacement studies and the level of TSPO expression was assessed using immunohistochemical analysis in syngeneic and allogeneic 9L rat glioma models.

Materials and methods

Radiochemicals and chemicals

Ready-to-inject, >99% radiochemically pure L-[11C]methionine ([11C]MET, (S)-2-amino-4-([11C]methylsulfanyl)-butanoic acid) was prepared from cyclotron-produced [11C] carbon dioxide (Cyclone 18/9 cyclotron, IBA, Louvain-la-Neuve, Belgium) on the basis of already published conditions using a commercially available TRACERLab™ FX-C synthesizer (GEMS, Buc, France) [19].

Ready-to-inject, >99% radiochemically pure [18F]DPA-714 (N,N-diethyl-2-(2-(4-(2-[18F]fluoroethoxy)phenyl)-5,7-dimethylpyrazolo[1,5-a]pyrimidin-3-yl)acetamide) was prepared from cyclotron-produced [18F]fluoride (Cyclone 18/9 cyclotron, IBA, Louvain-la-Neuve, Belgium) on the basis of already published standard conditions [20] using a commercially available TRACERLab™ FX-FN synthesizer (GEMS, Buc, France) [21], a process which was formerly performed on a

Zymate XP robotic system (Zymark, Hopkinton, MA, USA) [22]. Radiolabelling of DPA-714 with 18F (half-life 109.8 min) uses a tosyloxy-for-fluorine nucleophilic aliphatic substitution (one-step process) and its preparation includes the following five stages: (1) dilution of the no-carrier-added, dried (activated) K[18F]F-Kryptofix® 222 complex (prepared from [18F]fluoride, potassium carbonate and Kryptofix® 222) with 700 μl of dimethyl sulphoxide (DMSO) containing 3.5–4.5 mg of the tosyloxy precursor for labelling (N,N-diethyl-2-(2-(4-(2-toluenesulfonyloxyethoxy)phenyl)-5,7-dimethylpyrazolo[1,5-a]pyrimidin-3-yl)acetamide); (2) heating the reaction mixture at 160°C for 5 min; (3) dilution of the reaction mixture with the HPLC mobile phase and pre-purification on a Sep-Pak® Alumina N™ cartridge; (4) HPLC purification on a semi-preparative Waters XTerra™ C18 column [eluent 0.1 M aq. ammonium acetate (pH 10)/acetonitrile: 60/40 (v:v)]; and (5) Sep-Pak® Plus C18 cartridge-based removal of the HPLC solvents. [18F]DPA-714, as an ethanolic (15%) physiological saline (aq. 0.9% NaCl) solution (6.7- to 8.5-GBq batches, 10-ml volume), is routinely obtained within 50–55 min starting from 35 GBq of [18F]fluoride (19–24% non-decay-corrected overall isolated yields) with specific radioactivities ranging from 74 to 222 GBq/μmol. Quality controls were performed on an aliquot of the ready-to-inject [18F]DPA-714 preparation, in compliance with our in-house quality control/assurance specifications

Solutions of (R,S)-PK11195 for i.v. injection were prepared by dissolving 2–3 mg of the compound in DMSO (0.2 ml), followed by dilution with PEG 400 (1 ml) and finally physiological saline (aq. 0.9% NaCl, 2 ml). Similarly, solutions of unlabelled DPA-714 for i.v. injection were prepared by dissolving 2–3 mg of the compound in DMSO (0.2 ml), followed by dilution with PEG 400 (0.4 ml) and finally physiological saline (aq. 0.9% NaCl, 1.2 ml). Both solutions were systematically freshly prepared on the day of the in vivo experiment, stored at room temperature and used within 2 h.

Cell cultures

The rat 9L and C6 as well as the mouse GL261 glioma cell lines were maintained in culture using Dulbecco's modified Eagle's medium (DMEM, Life Technologies®, Karlsruhe, Germany) containing 10% fetal bovine serum (FBS, Roche Diagnostics®, Mannheim, Germany) and 1% antibiotics (penicillin/streptomycin, Life Technologies®) and were grown at 37°C in a humidified atmosphere of 5% CO_2.

Animal model

All experiments were performed under an animal use and care protocol approved by the Animal Ethics Committee, and they were conducted in accordance with the European Union regulations on animal research.

9L rat glioma cells were stereotactically implanted in the striatum of Fischer ($n=5$), Wistar ($n=8$) and Sprague Dawley ($n=5$) rats. Intracranial 9L tumours were established by injection of 2×10^5 9L cells (in 1 μl DMEM) into the right striatum using a Hamilton syringe in a stereotactic apparatus (Stoelting). Cells were slowly infused (200 nl/min) and the syringe was left in place after injection for an additional 5 min before it was retracted slowly. The coordinates used were 4 mm lateral to the bregma and 5 mm in depth to the dural surface.

Magnetic resonance imaging (MRI)

All scans were performed on a horizontal bore, 7 T Pharma-Scan Bruker imaging system equipped with gradients with a maximum strength of 760 mT/m. A 3.6-cm ID quadrature radiofrequency (RF) coil was used for transmission and reception. Scout scans and anatomical images were acquired to localize the tumours. We ensured good B0 homogeneity through automatic iterative FASTMAP methods (ParaVision 5.1). T2-weighted images were acquired using a fast spin-echo sequence [effective echo time (TE_{eff})=60 ms, acceleration factor 8, repetition time (TR)=3,000 ms, field of view (FOV) 2.56×2.56 cm^2, matrix size 128×128, slice thickness 0.3 mm, 8 averages, acquisition time 3 min 24 s]. During the MRI acquisition the animals were anaesthetized with 2% isoflurane in air administered using a nose cone. We monitored the respiration rate and maintained the body temperature at 37°C.

PET scan and data acquisition

To monitor tumour growth by PET in vivo, L-[S-methyl-^{11}C]methionine ([^{11}C]MET) as well as [^{18}F]DPA-714 dynamic PET scans were acquired 11–14 days post-inoculation. The injected doses were 2.70±0.66 mCi (mean±SD) and 1.44±0.34 mCi (mean±SD) for [^{11}C]MET and [^{18}F]DPA-714, respectively. Imaging was performed on a Siemens Focus 220 microPET scanner. [^{11}C]MET PET was performed in selected animals. Animals were anaesthetized with isoflurane (induction: 4%, maintenance: 2–2.5%) in a mixture of 100% O$_2$. During PET imaging, the rat's head was fixed in a home-made stereotactic frame compatible with PET acquisition. Rats were kept normothermic using a heating blanket (Homeothermic Blanket Control Unit, Harvard Apparatus Edenbridge, Kent, UK). Radiolabelled compounds and unlabelled ligands [PK11195 ($n_{1 \text{ mg/kg}}=5$, $n_{5 \text{ mg/kg}}=4$); DPA-714 ($n_{1 \text{ mg/kg}}=7$, $n_{5 \text{ mg/kg}}=4$)] were injected into the caudal vein through a 24-gauge catheter. PET data were acquired during 60 min for [^{11}C]MET and 70 min for [^{18}F]DPA-714, following radiotracer injection. For in vivo displacement studies one PET scan of 70 min was performed where radiolabelled compounds were injected at the start of the PET acquisition and unlabelled compounds were injected at 1.0 and 5.0 mg/kg

30 min after injection of the radiotracers. The acquisition protocol used the following parameters: the time coincidence window was set to 6 ns and the levels of energy discrimination were set to 350 and 750 keV. The data files acquired in list mode were histogrammed into 3-D sinograms with a maximum ring difference of 47 and span of 3. For [^{11}C]MET, the list-mode data of the emission scans were sorted into 18 frames. For [^{18}F]DPA-714, the list-mode data were sorted into 24 dynamic frames or into 29 dynamic frames for displacement studies in order to better define the displacement time course. Two different methods were used to obtain the attenuation correction factors: (1) for [^{11}C]MET experiments a transmission scan was performed prior to radiotracer injection using an external ^{68}Ge point source and (2) for [^{18}F]DPA-714 experiments segmentation of the emission map was used to calculate the attenuation map as reported previously [18, 23]. Finally, the emission sinograms (i.e. each frame) were normalized, corrected for scatter, attenuation and radioactivity decay and reconstructed using Fourier rebinning (FORE) and 2-D ordered subset expectation maximization (OSEM) (16 subsets and 4 iterations).

Image analysis and modelling

PET image analysis was performed using VINCI, a fast graphical image analysis package [24] with image coregistration tools. The Anatomist BrainVISA software package (http://www.brainvisa.info) was also used for data evaluation. PET images were coregistered to the corresponding MRI. For quantitative analysis a volume of interest (VOI) analysis was performed on kinetic as well as summed image data sets. A VOI was manually delineated on the tumour, and as reference region a mirror VOI was copied and symmetrically pasted into the contralateral hemisphere. For this, we first automatically reoriented the summed PET image so as to realign the inter-hemispheric plane with the centre plane of the image grid. This procedure was equivalent to computing the transformation defining an appropriate plane to split the brain into two roughly symmetric parts and then realigning this plane—defined as the mid-sagittal plane—with the centre of the image lattice. We then applied this previously computed transformation to the VOI (outlined on non-reoriented PET) and flipped the resampled VOI with respect to the centre plane of the image grid (i.e. the plane best superposing the two hemispheres of the brain by reflective symmetry). A visual inspection of the VOI transformation assured VOI placement in the contralateral brain hemisphere. In order to investigate another reference region we also manually defined a VOI in the cerebellum, which is frequently used as a reference region in clinical [^{11}C]PK11195 or [^{123}I]iodo-PK11195 studies of Alzheimer's disease [25–27].

For PET data modelling, the simplified reference tissue model (SRTM) [28] from the PMOD software package

(version 2.5, PMOD Technologies Ltd., Zurich, Switzerland) was used to assess the BP in the target VOI. This model relies on a two-tissue reversible compartment for the target region (here tumour VOI) and a single-tissue compartment for the reference volume (here contralateral or cerebellum). Three parameters were estimated for each kinetic: R_1 (K_1/K'_1), which represents the ratio of tracer delivery; k_2, which is the clearance from the target tissue back to the vascular compartment; and BP_{ND} (k_3/k_4), which is the binding potential of the tracer to the tissue and refers to ratio of specifically bound radioligand to that of non-displaceable radioligand in tissue at equilibrium [29]. In order to evaluate the impact of R_1 on the BP_{ND} we recalculated the generated kinetic modelling files in the kinetic modelling tool of PMOD and manually set R_1 values equal to 1 with unchanged k_2 and BP_{ND} values before recalculation of simulated curve fits. This method was previously described for the TSPO radioligand [^{11}C] DPA-713 [30] to evaluate the impact of flow effects on the measured BP_{ND}.

Western blot

Proteins were extracted from 9L, C6 and GL261 cultured cell suspensions. Cells were lysed in buffer containing 50 mM Tris-HCl pH 7.5, 1% (v/v) NP40, 0.5% (w/v) sodium deoxycholate, 50 mM NaPPi, 100 mM NaF, 5 mM Na_3VO_4, 150 mM NaCl and protease inhibitor mix (Roche Diagnostics GmbH, Mannheim, Germany). The amount of protein present in each sample was quantified using a BCA Protein Assay (Pierce, Rockford, IL, USA). Equal amounts (10 μg) of denatured (95°C, 5 min) protein were separated using sodium dodecyl sulphate polyacrylamide gel electrophoresis (SDS-PAGE) and blotted to polyvinylidene difluoride (PVDF) membrane (Amersham Pharmacia Biotech, Freiburg, Germany) in standard Tris-glycine transfer buffer. After blocking of non-specific binding sites with 3% bovine serum albumin (BSA) or 3% non-fat dry milk in 0.2% phosphate-buffered saline (PBS)-Tween 20 (PBST) for 2 h at room temperature the membrane was washed three times with PBST. Incubation with the primary antibodies diluted in PBST with 3% of BSA for the anti-TSPO antibody and 3% non-fat dry milk for the anti-β-actin antibody, respectively (1/10,000 dilution of the anti-rat TSPO antibody NP155 [31] generously provided by Dr. M. Higuchi, NIRS, Japan, and 1/5,000 dilution of the anti-β-actin antibody purchased from Sigma Aldrich), was performed overnight at 4°C. After three wash steps, the membrane was incubated with the appropriate secondary antibody (1/2,000 dilution) in 1% of BSA or 1% non-fat dry milk in PBST for 1 h at room temperature. After three 10-min wash sessions, the membrane was then developed using an Amersham ECL Plus Western Blotting System (GE Healthcare Life Sciences) onto

films. Western blots were normalized using the anti-β-actin antibody.

Immunohistochemistry

For immunohistochemical labelling, brains of tumour-bearing animals were frozen in isopentane and stored at −80°C. Coronal brain sections of 5 μm thickness were prepared on a cryostat and were treated as reported previously [32]. Sections were incubated with primary antibodies [rabbit anti-rat TSPO antibody NP155, 1:1,000 generously provided by Dr. M. Higuchi, NIRS, Japan, mouse anti-rat CD11b, 1:300 (Serotec, Raleigh, NC, USA) and chicken anti-rat glial fibrillary acidic protein (GFAP), 1:500 (Abcam)] at room temperature for 1 h. The excess antibody was removed by three consecutive wash cycles with PBS. Then the appropriate secondary antibodies coupled with fluorophores (goat anti-rabbit IgG with Alexa Fluor 488 nm for the rat anti-TSPO antibody NP155, goat anti-mouse IgG with Alexa Fluor 594 nm for CD11b and goat anti-chicken IgG with Alexa Fluor 647 nm for the anti-GFAP antibody) or horseradish peroxidase (HRP) (goat anti-rabbit IgG for the rat anti-TSPO antibody NP155) were added to each slide for 30 min, following by another three washes with PBS. On each slide, one small tissue section incubated with the secondary antibody without the primary antibody served as controls. Finally, the ProLong® gold antifade reagent with 4′-6′-diamidino-2-phenylindole (DAPI) (purchased from Invitrogen) was added to stain the cell nuclei and mount the slide. Fluorescent microscopy was performed using a Zeiss AxioCam with a HXP 120 module (Carl Zeiss S.A.S.).

Statistical analysis

Differences between the three rat strains in the tumour volume versus contralateral brain hemisphere were analysed using one-way analysis of variance, and Bonferroni's multiple comparison tests were used for post hoc analysis (GraphPad Prism, GraphPad Software Inc.).

Results

TSPO expression in glioma cell lines and in 9L glioma

Western blot results demonstrated a level of TSPO expression in 9L cells similar to that in rat C6 glioma cells (Fig. 1a), which served as positive controls [33, 34]. In contrast, murine glioma GL261 cells did not show significant expression of TSPO. Histology and
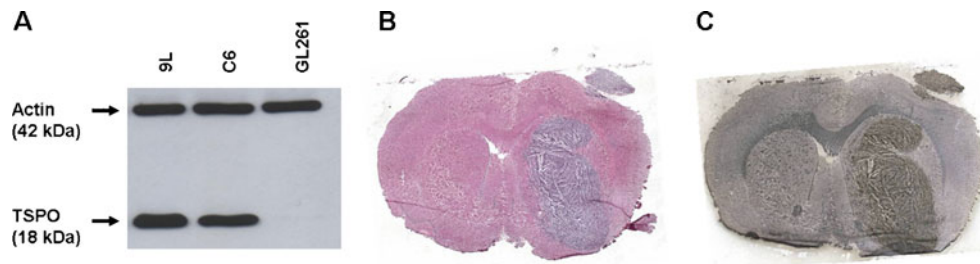
Fig. 1 **a** Expression levels of TSPO measured in protein extracts from rat and murine glioma cell lines (9L, C6 and GL261). Western blots were normalized using the anti-β-actin antibody. H&E staining (**b**) and immunohistochemistry for TSPO (**c**) of coronal brain sections illustrating tumour growth and high level of TSPO expression in a 9L glioma

immunohistochemistry of intracranially growing 9L rat gliomas demonstrated clear tumour growth [haematoxylin and eosin (H&E) staining; Fig. 1b] and strong TSPO expression (anti-TSPO staining; Fig. 1c).

In vivo imaging of 9L glioma

To monitor tumour growth in vivo, T2-weighted MRI and [11C]MET PET were performed prior to [18F]DPA-714 PET imaging. 9L glioma cell inoculation resulted in tumour growth as evidenced by T2-weighted MRI and [11C]MET PET (Fig. 2a). [18F]DPA-714 PET images were coregistered to the corresponding MRI and demonstrated significant [18F]DPA-714 accumulation at the site of tumour implantation (Fig. 2a). MRI and [18F]DPA-714 PET imaging of

sham-operated animals did not demonstrate any significant [18F]DPA-714 accumulation at the site of the needle tract (Fig. 2b).

Quantitative analysis of [18F]DPA-714 uptake in 9L glioma in vivo

9L cell implantation in (1) syngeneic Fischer rats, (2) allogeneic Wistar rats [35] and (3) Sprague Dawley rats resulted in tumour growth in all strains. Although all three rat strains manifested significant [18F]DPA-714 PET uptake in the tumour as compared to the contralateral site or cerebellum, time-activity curves (TACs) as well as calculation of %ID/cc showed significant differences between tumour and contralateral region or tumour and cerebellum in all strains (Fig. 3;
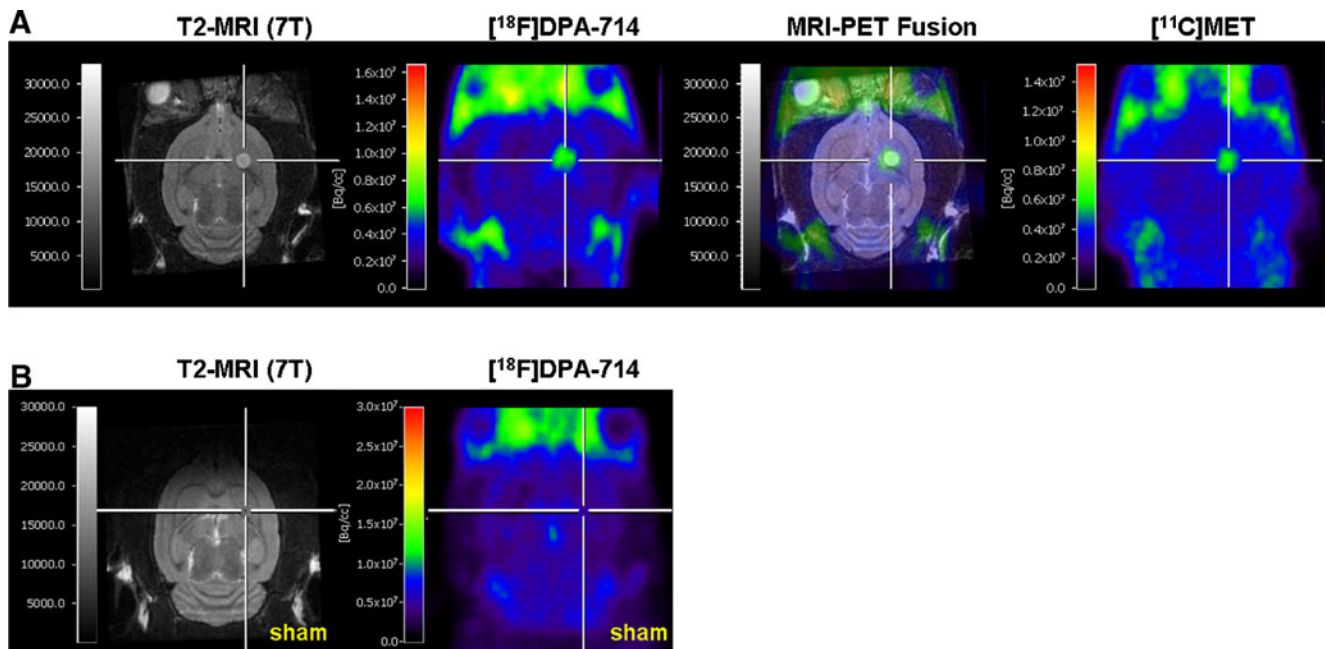

Fig. 2 T2-weighted MRI and PET imaging of animals bearing i.c. 9L rat glioma (**a**) and sham-operated animals (**b**). T2-weighted MRI and summed [11C]MET PET images (0–60 min) illustrate tumour growth; summed [18F]DPA-714 PET images (0–70 min) demonstrate significant tracer uptake in tumour as compared to the contralateral site (**a**). [18F]DPA-714 PET image of a sham-operated animal shows no important [18F]DPA-714 uptake at the site of the needle tract
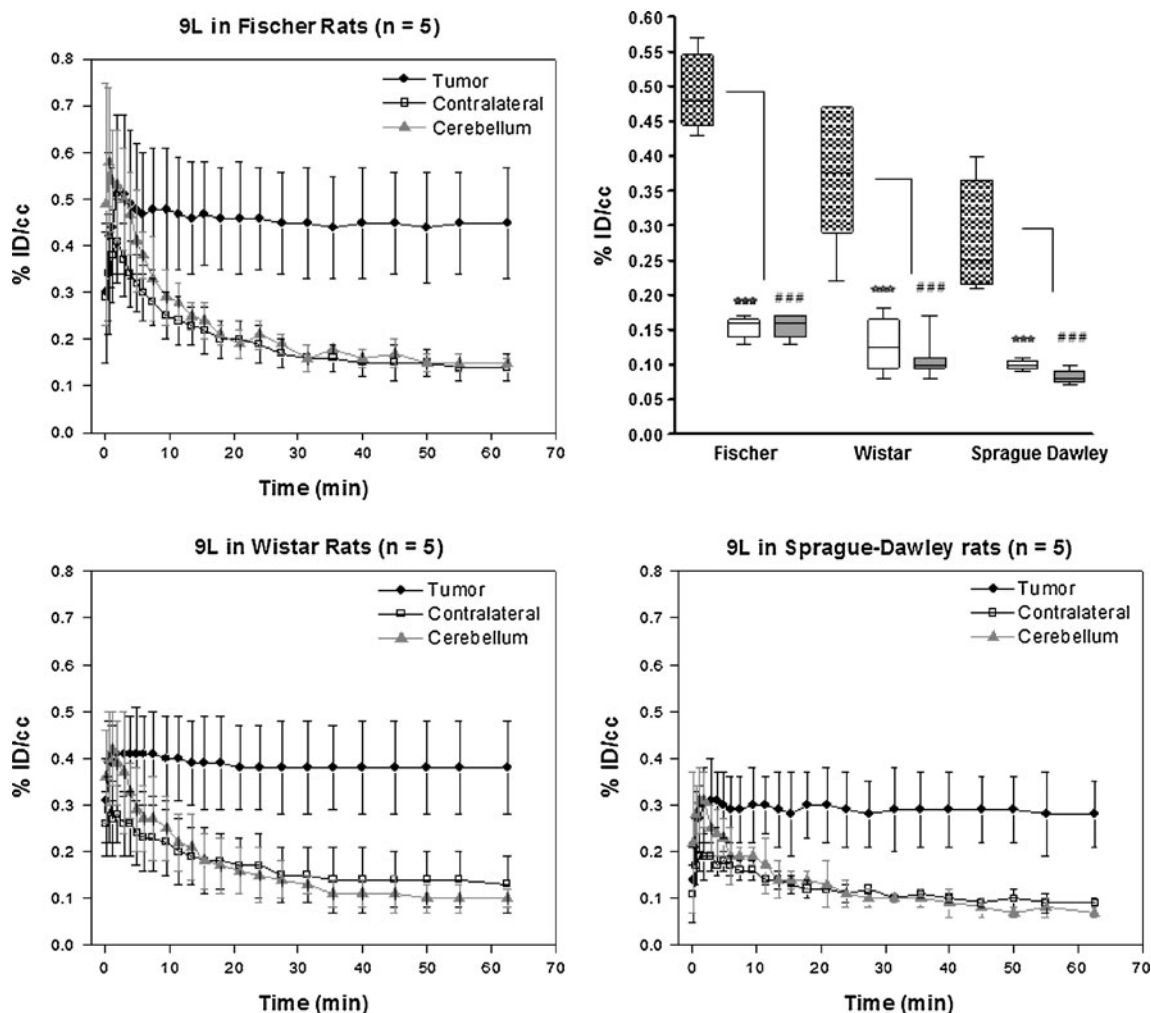
Fig. 3 TACs of a VOI placed on the tumour and the contralateral hemisphere for [18F]DPA-714 in Fischer (n=5), Wistar (n=8) and Sprague Dawley (n=5) rats. Box plot of corresponding VOI analysis shows significant differences in [18F]DPA-714 uptake in tumour vs control (***p<0.001) or cerebellum (###p<0.001) in all strains. VOI analysis was performed on summed images over the last 30 min of the PET scan

p<0.001). Mean [18F]DPA-714 uptake in the tumour was 0.49±0.05%ID/cc, 0.37±0.10%ID/cc and 0.28±0.08%ID/cc in Fischer, Wistar and Sprague Dawley rats, respectively (Fig. 3, box plot). Calculation of control VOIs in the contralateral hemisphere resulted in [18F]DPA-714 uptake values of 0.15±0.02%ID/cc (Fischer), 0.13±0.04%ID/cc (Wistar) and 0.10±0.01%ID/cc (Sprague Dawley). Similar results were obtained using the cerebellum as control region (0.16±0.02%ID/cc (Fischer), 0.11±0.03%ID/cc (Wistar) and 0.08±0.01%ID/cc (Sprague Dawley). Representative [18F]DPA-714 TACs of tumour and corresponding model fits (simplified reference tissue model) for individuals of the three rat strains are illustrated in Fig. 4. TACs of standardized uptake values (SUVs, %ID/cc per kg) demonstrate significantly higher uptake of [18F]DPA-714 in the tumour versus contralateral region or cerebellum [p<0.001 in Fischer and Wistar, p<0.01 in Sprague Dawley rats (data not shown)]. TACs of the two reference regions appear

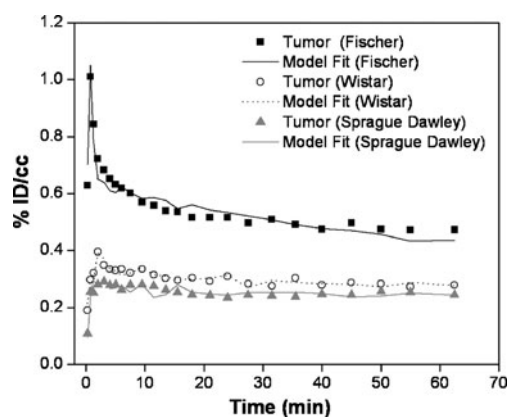similar although differences exist within the first 10 min of the PET scan. Mean uptake values±SD in tumour were

Fig. 4 Representative [18F]DPA-714 TACs and model fits (SRTM) for tumour of a Fischer (*black square*), a Wistar (*open circle*) and a Sprague Dawley rat (*triangle*)

2.18±0.34, 1.16±0.32 and 0.67±0.23 in Fischer, Wistar and Sprague Dawley rats, respectively. SUVs of control regions did not differ significantly between the Fischer (0.66±0.08 contralateral versus 0.68±0.07 cerebellum), Wistar (0.41±0.15 contralateral versus 0.33±0.08 cerebellum) or Sprague Dawley strains (0.23±0.03 contralateral versus 0.19±0.01 cerebellum).

Kinetic modelling

Kinetic modelling of the PET data using the SRTM [28] estimated the BP_{ND} (binding potential), R_1 (ratio of tracer delivery) and k_2 (efflux constant) values. A VOI placed in the contralateral mirror region to the tumour and a VOI placed in the cerebellum were compared as reference regions in SRTM. The BP_{ND} for [^{18}F]DPA-714 using the contralateral VOI as reference region was similar in the three different rat models (mean values±SD were 2.17±0.53, 2.05±0.96 and 2.03±0.48 in Fischer, Wistar and Sprague Dawley rats, respectively) (Table 1). Corresponding R_1 values for [^{18}F]DPA-714 were close to 1 (1.24±0.19, 1.33±0.17 and 1.42±0.31 for Fischer, Wistar and Sprague Dawley rats) and did not show significant differences between strains. No differences were found either for k_2, the clearance from the target tissue back to the vascular compartment: 0.15±0.07, 0.16±0.06 and 0.12±0.07 min^{-1}, for Fischer, Wistar and Sprague Dawley rats, respectively. Since R_1 values were higher than 1, we recalculated simulated TACs after imposing an R_1 value of 1, in order to investigate the influence on the BP_{ND}. With R_1=1 BP_{ND} values for the three rat strains were not significantly different from those obtained using the non-imposed R_1 (Fischer: 2.17±0.53 vs 2.00±0.52, $p>0.05$; Wistar 2.05±0.96 vs 1.75±0.52, $p>0.05$; and Sprague Dawley 2.03±0.48 vs 1.70±0.44, $p>0.05$). Using the cerebellum as reference region, no significant differences were found

when comparing R_1, k_2 or BP_{ND} values between the different rat strains. Furthermore, comparing the values calculated with the cerebellum as reference region, BP_{ND} and k_2 did not differ significantly from those obtained with the contralateral region as reference region. However, calculated R_1 values in Fischer rats using cerebellum as reference region were significantly smaller compared to those obtained with contralateral VOI as reference region ($p<0.05$). The same differences were found for R_1 values in Wistar and Sprague Dawley rats when using the cerebellum versus the contralateral site as reference region (both $p<0.001$).

In vivo displacement studies

In vivo displacement studies by administration of 1 and 5 mg/kg of either unlabelled DPA-714 or the reference compound PK11195, 30 min after tracer injection, resulted in a significant reduction in the tumour radioactivity concentrations (p values for displacement with 1 or 5 mg/kg of DPA-714 were $p<0.01$ and $p<0.001$, respectively; and for displacement with 1 or 5 mg/kg of PK11195, p values were $p>0.05$ and $p<0.05$, respectively; Fig. 5). Injection of 1 mg/kg of unlabelled compounds reduced the radiotracer uptake to 62 and 74% of its pre-displacement value, respectively (Table 2). Accordingly, administration of higher amounts of unlabelled DPA-714 or PK11195 (5 mg/kg) induced stronger displacements resulting in 15 and 45% of radiotracer uptake in the tumour compared to pre-displacement values (Table 2). PET images and mean TACs (Fig. 6) showed a rapid and nearly complete displacement of [^{18}F]DPA-714 after injection of DPA-714, and radioactivity concentration in the tumour area decreased to a level similar to that measured in the contralateral brain area. Displacement with an excess of PK11195 also demonstrated a significant level of displaceable binding, although lower than with DPA-714.

Table 1 R_1, k_2 and BP_{ND} values obtained from [^{18}F]DPA-714 PET data in Fischer, Wistar and Sprague Dawley rats using contralateral site or cerebellum as reference region

	Fischer	Wistar	Sprague Dawley
Number of rats	n=5	n=8	n=5
R_1 (reference region contralateral)	1.24±0.19	1.39±0.27	1.42±0.31
R_1 (reference region cerebellum)	0.88±0.12*	0.91±0.16***	0.82±0.24***
k_2 (reference region contralateral)	0.15±0.07	0.16±0.06	0.12±0.07
k_2 (reference region cerebellum)	0.14±0.09	0.09±0.03	0.11±0.03
BP_{ND} (reference region contralateral)	2.17±0.53	2.05±0.96	2.03±0.48
BP_{ND} (reference region cerebellum)	2.03±0.53	2.55±0.79	2.24±1.11

Results are expressed as mean values±SD. No significant differences were found when comparing R_1, k_2 or BP_{ND} values between the different rat strains; however, R_1 values from Fischer, Wistar and Sprague Dawley rats were significantly different depending on the reference region selected for calculations in SRTM. The calculated R_1 value in Fischer rats using cerebellum as reference region was significantly smaller as compared to contralateral VOI as reference region (*$p<0.05$). The same is true for R_1 values in Wistar and Sprague Dawley rats comparing cerebellum and contralateral site as reference region (both ***$p<0.001$). No significant differences were found for k_2 or BP_{ND} comparing the two reference regions

R_1 ratio of tracer delivery, k_2 efflux constant, BP_{ND} binding potential. Results are expressed as mean values±SD
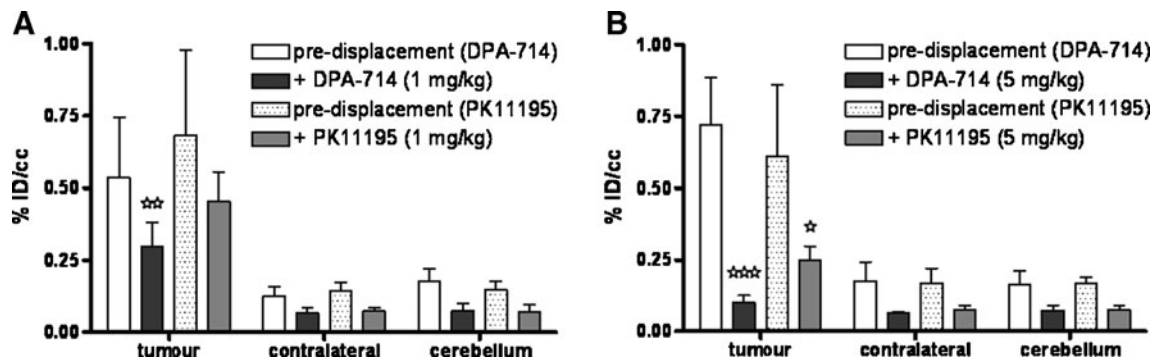
Fig. 5 In vivo displacement of $[^{18}F]DPA$-714 by injection of DPA-714 or PK11195 with 1 mg/kg (**a**) and 5 mg/kg (**b**), respectively. Graphs illustrate %ID/cc values before versus after administration of the unlabelled compound in tumour and control VOIs. Measurements for pre- and post-displacement were compared at 27.5 and 47.5 min after radiotracer injection, two time points with identical frames of PET data acquisition. $[^{18}F]DPA$-714 uptake decreased significantly in the tumour VOI after displacement with DPA-714 at 1 mg/kg (**p<0.01) and 5 mg/kg (***p<0.001) or with 5 mg/kg PK11195 (*p<0.05)

Immunohistochemistry

In order to analyse TSPO expression at the cellular level we performed immunofluorescence labelling of TSPO in the rat 9L gliomas. Tumours grown intracerebrally showed complex tissue composition, comprising cancerous cells as well as cells of the tumour microenvironment (TME) such as endothelial cells, vessels and cells of the immune system such as glioma-infiltrating microglia/macrophages [36]. Since it is known that TSPO expression is dramatically increased upon activation of glial cells, we performed triple immunostaining for TSPO, CD11b and GFAP to investigate separately TSPO expression in activated glioma-infiltrating microglia/macrophages or astrocytes and in 9L glioma cells. Previous data have suggested that systemic macrophages are the predominant inflammatory cells infiltrating gliomas [37, 38]. However, since the origin of tumour-associated microglia/macrophages has not yet been fully determined [39] labelling with CD11b reflects both resident microglia as well as glioma-infiltrating macrophages. A panoramic view of TSPO immunofluorescence demonstrates that TSPO expression was mostly restricted within the tumour (Fig. 7a), confirming the PET results. CD11b immunolabelling revealed the presence of microglial/macrophage cells within the tumour, whereas GFAP staining did not show the presence of astrocytes in the tumour. Higher magnification showed a high level of TSPO expression in activated microglial/macrophage cells. Although the bulk expression of TSPO originated from glioma cells, these results clearly demonstrate that the TSPO signal derived in vivo originates from both cancerous and immune cells (Fig. 7b).

Discussion

The present study evaluated the potential use of the TSPO radioligand $[^{18}F]DPA$-714 as a PET imaging marker for non-invasive imaging of intracranial rat glioma models in vivo. $[^{18}F]DPA$-714 PET imaging of 9L gliomas grown in three different rat strains (Fischer, Wistar and Sprague Dawley rats) demonstrated significant $[^{18}F]DPA$-714 PET uptake at the site of tumour implantation as compared to the contralateral brain hemisphere or cerebellum, and in vivo displacement studies with unlabelled DPA-714 or PK11195 showed high specificity of $[^{18}F]DPA$-714 for TSPO. Finally, immunohistochemistry of brain/tumour sections confirmed high TSPO expression within the glioma and demonstrated the presence of TSPO-positive glioma as well as TSPO-positive microglial cells (Fig. 7).

The gold standard imaging method for the diagnosis of human gliomas is T1-weighted MRI with and without gadolinium enhancement in conjunction with T2-weighted MRI. These sequences provide information on the size and localization of the tumour and additional information about secondary phenomena such as disruption of the blood-brain barrier, mass effect, perifocal oedema, haemorrhage, necrosis and signs of increased intracranial pressure [40]. However, no specific information about the biological or metabolic activity of the tumour is provided by T1- or T2-weighted MRI. Recent reviews point out the usefulness of combining advanced

Table 2 In vivo displacement of $[^{18}F]DPA$-714 using 1 or 5 mg/kg of DPA-714 or PK11195

	Tumour	Contralateral	Cerebellum
+ DPA-714			
1 mg/kg	62.3±27.6	56.3±9.2	46.4±5.0
5 mg/kg	14.5±0.4	35.4±7.9	44.5±11.7
+ PK11195			
1 mg/kg	74.0±24.3	51.3±5.9	49.0±5.2
5 mg/kg	44.8±13.0	46.6±11.9	44.6±8.7

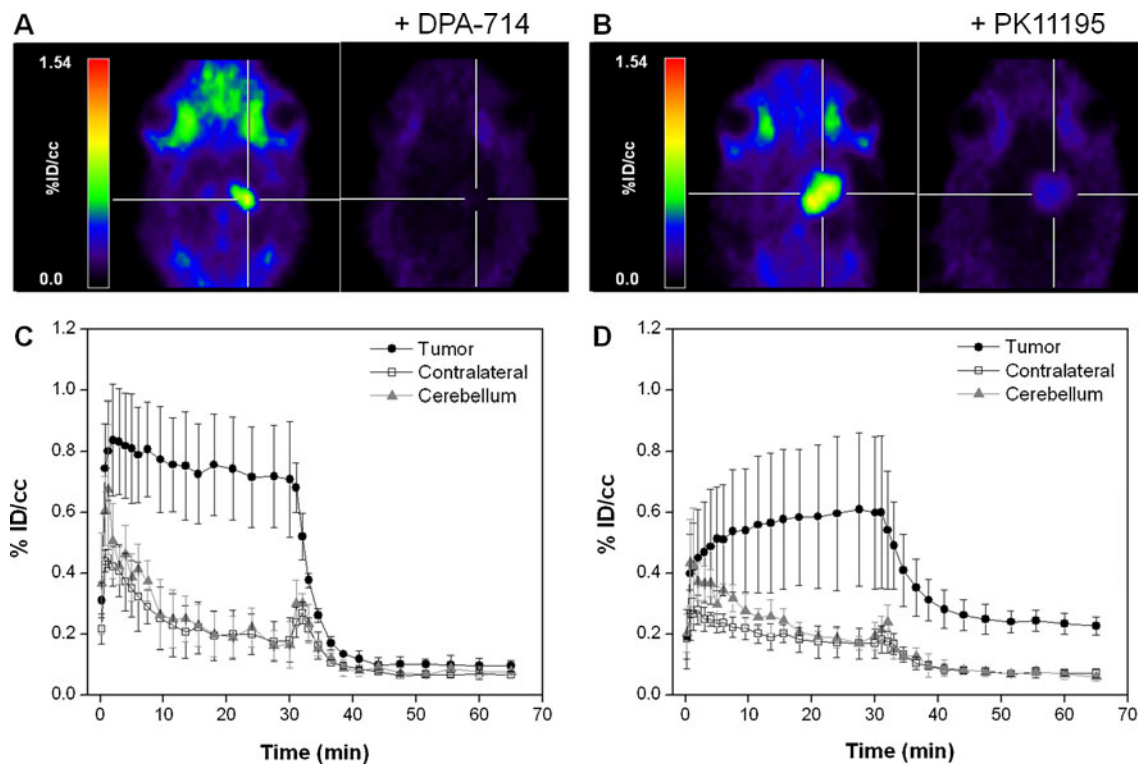Results are expressed as % of radiotracer uptake of pre-displacement value

Fig. 6 Summed [^{18}F]DPA-714 PET images before (0–30 min) and after (40–70 min) in vivo displacement with 5 mg/kg DPA-714 (**a**) or PK11195 (**b**). TACs for [^{18}F]DPA-714 in tumour and control VOI after injection of DPA-714 (**c**) or PK11195 (**d**)

imaging methods, in particular PET in conjunction with MRI, to visualize additional molecular information and biological changes of the tumour [41, 42]. Overexpression of TSPO has been reported in a variety of cancer cell lines and human tumours including glioma [8], and clinical studies using the TSPO radioligand [^{11}C]PK11195 imaged human glioma using PET [10, 17]. However, this radioligand has various limitations, among others, the labelling with ^{11}C ($T_{1/2}$: 20.4 min) restricts its extensive clinical use [2]. In the last few years many efforts have been undertaken in the development of new TSPO radioligands. One of the [^{11}C]PK11195 challengers that showed improved characteristics when compared to the reference compound is the pyrazolo[1,5]pyrimidine [^{18}F]DPA-714 [20]. In a rat model of neuroinflammation, [^{18}F]DPA-714 was directly compared to [^{11}C]PK11195 and another pyrazolo[1,5]pyrimidine [^{11}C]DPA-713 [18] and demonstrated improved signal to noise ratio and increased BP as compared to [^{11}C]PK11195. Martín et al. used this TSPO radioligand to characterize the time course of TSPO expression in an animal model of focal cerebral ischaemia [32]. Other new TSPO radioligands reported include the phenoxyarylacetamides [^{11}C]DAA1106, [^{11}C]PBR28 or [^{18}F]PBR06, which have been claimed to perform better than [^{11}C]PK11195 for in vivo imaging of TSPO, based on higher binding affinity in an animal model of neuroinflammation [43] and high levels of specific binding in non-human primates and in human brain [44, 45]. The new TSPO ligands may redraw attention to TSPO

PET imaging of gliomas, as suggested by a recent study of in vivo imaging of [^{18}F]PBR06 in a preclinical model of glioma [33].

Here we demonstrate that 9L glioma cells as well as intracranial 9L gliomas express TSPO at a high level. In vivo PET imaging of [^{18}F]DPA-714 in the 9L glioma model resulted in high [^{18}F]DPA-714 uptake in the tumour as compared to the contralateral brain hemisphere. Comparison with sham-operated animals shows that the PET signal was not influenced by an uptake of [^{18}F]DPA-714 due to a neuroinflammatory reaction induced by the operation procedure itself (Fig. 2).

TACs for tumour VOIs demonstrate a slow washout of [^{18}F]DPA-714 as compared to control brain regions, as previously reported in a rat model of focal cerebral ischaemia [32]. Slow washout may also be a characteristic of the rat glioma model. Using [^{18}F]PBR06 in a C6 glioma model in Wistar rats, Buck et al. also demonstrated a slower washout of this radioligand from the tumour tissue than from the contralateral brain, thus facilitating a strong tumour to contralateral brain contrast [33].

The 9L glioma originates from a tumour that arose in Fischer rats [46]. However, 9L cells can also form tumours in allogeneic Wistar [35] and Sprague Dawley rats [47]. Quantitative data analysis demonstrated that [^{18}F]DPA-714 uptake was significantly enhanced in the tumour as compared to the contralateral brain hemisphere or cerebellum in
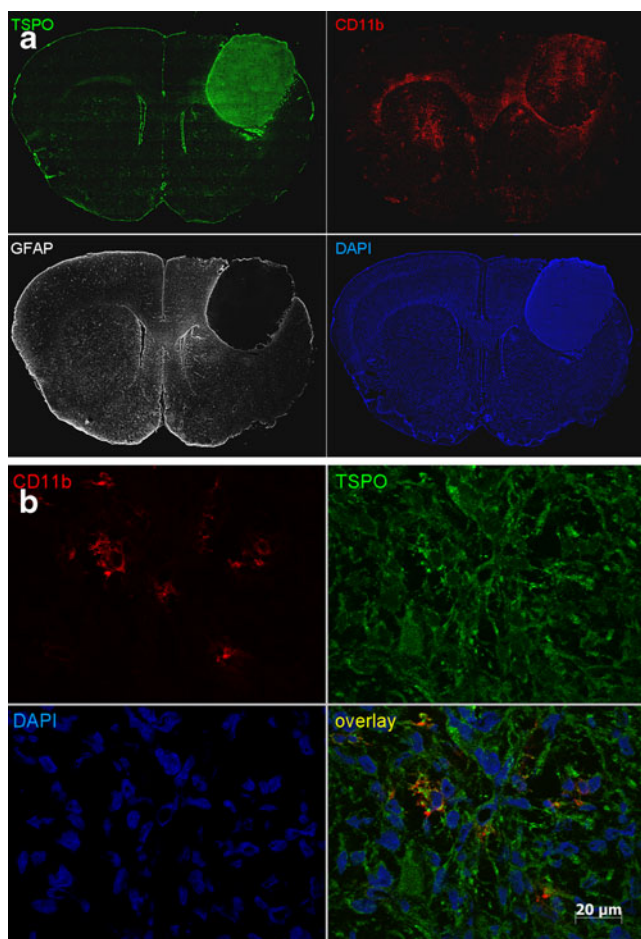
Fig. 7 Immunohistochemistry of TSPO (*green*), CD11b (*red*) and GFAP (*white*) on whole coronal brain sections of animals bearing i.c. 9L glioma (**a**) illustrates strong TSPO expression and the presence of CD11b-positive microglial/macrophage cells in the tumour. In contrast, GFAP staining did not reveal the presence of astrocytes within the glioma. Triple labelling at higher magnification (**b**) shows a number of CD11b-positive microglia/macrophages present in the tumour expressing a high level of TSPO. Nuclear counterstaining was performed using DAPI (*blue*)

all of the three strains. Furthermore, differences in the radioactivity concentrations expressed in %ID/cc or SUVs in the tumour were observed between the different rat strains regardless of body weight. An explanation for the differences in the %ID/cc values in the tumour may result from the tumour model itself. Since 9L cells are allogeneic to Wistar or Sprague Dawley rats, the tumours may present different stages of carcinogenesis and thus e.g. express proteins at different levels, as previously shown for K (ATP) and K(Ca) channels when 9L tumours were compared in Wistar and Fischer rats [35]. Another factor that may influence specific radiotracer binding is the contribution of the TME, in particular the presence of inflammatory cells such as activated microglia, which may be different for 9L tumours in syngeneic or allogeneic rats. Inter-strain differences in radiotracer plasma availability (due to excretion,

metabolism or binding to plasma proteins) or differences in cerebral vascularization may also contribute to the differences measured in tumour radioactivity concentration. Wistar rats present a significantly greater number of proximal side branches of the long proximal middle cerebral artery segment than Fischer rats [48]. Since %ID/cc values represent a combination of free, specifically and non-specifically bound radioligand in a target region, we modelled PET data using the SRTM [28]. It should be noted that one of the requirements of SRTM is the use of a reference region without specific binding of the ligand. In order to normalize for inter-strain differences we performed our calculations using SRTM, although there is a small displaceable binding in both reference regions analysed in our study. Estimated R_1, k_2 and BP_{ND} values did not show significant changes between the rat strains independently of the reference region chosen, suggesting that the inter-strain differences are likely due to anatomical and/or radiotracer metabolism variations between strains. However, a difference was found for R_1 values, whether the contralateral side or the cerebellum were taken as reference region ($p<0.05$ and $p<0.001$ for Fischer and Wistar or Sprague Dawley rats, respectively, Table 1). This may be explained by the differences seen in particular for the first minutes of TACs, as R_1 defined as the ratio of tracer delivery (K_1/K_1') and K_1 and K_1', respectively, are mainly determined by the first minutes after radiotracer injection.

As R_1 values (K_1/K_1') calculated with the contralateral side as reference region were higher than 1 (1.24 ± 0.19, 1.33 ± 0.17 and 1.42 ± 0.31 for Fischer, Wistar and Sprague Dawley rats), indicating a facilitated entry of the radioligand into the tumour as compared to the reference region, we examined whether increased [^{18}F]DPA-714 uptake into the tumour may have been due to disruption of the blood-brain barrier. However, imposing a hypothetical R_1 value of 1 did not significantly influence the BP_{ND} values, indicating that [^{18}F]DPA-714 delivery into the tumour has only a limited effect on the BP_{ND}.

Accordingly, in vivo displacement studies demonstrated that [^{18}F]DPA-714 uptake reflects specific TSPO binding. Increasing amounts of unlabelled compound (DPA-714 or PK11195) yielded an increased displacement of tumour radioactivity concentrations. A dose of 5 mg/kg of unlabelled DPA-714 displaced more than 85% of the in vivo tumour uptake, whereas only 55% of the original tumour radioactivity concentration was displaced after administration of 5 mg/kg unlabelled PK11195 (Fig. 5b, Table 2). This difference in the displacement of the TSPO radioligand using the corresponding unlabelled compound or unlabelled PK11195 has previously been reported [32] and is likely due to a higher level of specific versus non-specific binding of DPA-714. It is most unlikely due to differences in affinities since in an in vitro binding assay, James et al. showed that affinities of DPA-714 and PK11195 for TSPO are comparable

[affinity of DPA-714 ($K_i=7.0\pm0.4$ nM); affinity of PK11195 ($K_i=9.4\pm0.5$ nM)] [20]. The differences in displacement efficiency may be explained by the fact that PK11195 is in a racemic form while DPA-714 is not. It is known that only the R-enantiomer of PK11195 is pharmacologically active, thus the displacing dose of PK11195 is half that of DPA-714.

Recently, PET studies using [11C]PBR28 demonstrated differences in affinity for TSPO in humans [49–51]. In a PET study with healthy human subjects, Fujita et al. reported the existence of non-binders for [11C]PBR28, whereas no such phenomenon has been described for [11C]PK11195 [49]. At a later date Owen et al. reported the presence of three different binding patterns with PBR28 (high-affinity binding, low-affinity binding and mixed-affinity binding), whereas no difference in affinity of PK11195 for TSPO was found in their study [51]. Furthermore, a recent study by the same group demonstrated that other TSPO ligands, currently used in clinical studies, can distinguish between these three binding patterns, although the differences in affinity do vary depending on the radioligand [52]. Strong differences were found for the phenoxyphenyl acetamides PBR28 and PBR06 (K_i ratio LAB to HAB: 55 and 17, respectively), whereas others like the phenylimidazopyridine PBR111, the phenylpyrazolopyrimidine DPA-713 or the phenoxyphenyl acetamide DAA1106 demonstrated only smaller differences in affinity (four- to fivefold). Although it is likely that [18F]DPA-714, which is an 18F-labelled derivative of DPA-713, will demonstrate a similar low difference in affinity ratio (low- versus high-affinity binding), this remains to be demonstrated.

In contrast to [11C]PBR28, PET studies with [18F]PBR06, [18F]PBR111, [11C]DPA-713 and [11C]DAA1106 did not report the phenomenon of low-affinity binding, probably due to an affinity for the respective PET radioligand sufficient to obtain a measurable PET signal [52]. At present the impact of these differences in binding affinity on the interpretation of the PET signal remains to be fully elucidated although it may be expected that low-affinity binding sites should lead to an underestimation of TSPO.

Gliomas are not exclusively composed of cancer cells but also of cells of the TME [36]. In particular, microglia/macrophages which can make up to 30% of the brain tumour mass [39] and astrocytes which are found in the proximity of glioma cells [53]. Increase in TSPO expression is a hallmark of glial cell activation upon neuroinflammation often associated with neoplastic processes. Thus, we tested whether activated microglia/macrophages and astrocytes contributed to the PET signal obtained in the glioma model using triple immunolabelling of brain/tumour sections. CD11b-positive microglia/macrophages were present within the glioma and demonstrated TSPO expression. In contrast, astrocytes were not found within the tumour and, thus, their contribution to the observed TSPO signal may be regarded

as limited. Although the majority of the TSPO signal within the tumour is provided by the glioma cells, activated microglia/macrophages contribute to the TSPO signal and thus to [18F]DPA-714 uptake in the tumour. In their in vivo imaging study using [18F]PBR06 in a rat glioma model, Buck et al. also demonstrated significantly higher TSPO immunostaining in the glioma as compared to normal brain tissue, and tumour to normal brain ratios were similar to TSPO protein levels in tumour tissue as compared to normal brain tissue [33]. However, no immunohistochemistry data about other cells possibly contributing to the PET signal were provided. The finding that microglia/macrophages account for the TSPO signal may be of limited importance for diagnostic purposes but may have significant implications when this radioligand is employed for assessment of treatment response to i.e. radiotherapy or combined radio- and chemotherapy.

Conclusion

This study demonstrates the feasibility of using PET imaging with the TSPO radioligand [18F]DPA-714 to characterize 9L glioma in vivo in different rat models. [18F]DPA-714 holds potential for imaging gliomas in patients if future clinical studies confirm the positive preclinical data reported here.

Conflicts of interest None.

References

1. Papadopoulos V, Baraldi M, Guilarte TR, Knudsen TB, Lacapère JJ, Lindemann P, et al. Translocator protein (18 kDa): new nomenclature for the peripheral-type benzodiazepine receptor based on its structure and molecular function. Trends Pharmacol Sci 2006;27 (8):402–9.
2. Chauveau F, Boutin H, Van Camp N, Dollé F, Tavitian B. Nuclear imaging of neuroinflammation: a comprehensive review of [11C] PK11195 challengers. Eur J Nucl Med Mol Imaging 2008;35 (12):2304–19.
3. Doorduin J, de Vries EF, Dierckx RA, Klein HC. PET imaging of the peripheral benzodiazepine receptor: monitoring disease progression and therapy response in neurodegenerative disorders. Curr Pharm Des 2008;14(31):3297–315.

4. Venneti S, Lopresti BJ, Wiley CA. The peripheral benzodiazepine receptor (translocator protein 18 kDa) in microglia: from pathology to imaging. Prog Neurobiol 2006;80(6):308–22.

5. Dollé F, Luus C, Reynolds A, Kassiou M. Radiolabelled molecules for imaging the translocator protein (18 kDa) using positron emission tomography. Curr Med Chem 2009;16(22):2899–923.

6. Scarf AM, Kassiou M. The translocator protein. J Nucl Med 2011;52(5):677–80.

7. Batarseh A, Papadopoulos V. Regulation of translocator protein 18 kDa (TSPO) expression in health and disease states. Mol Cell Endocrinol 2010;327(1–2):1–12.

8. Corsi L, Geminiani E, Baraldi M. Peripheral benzodiazepine receptor (PBR) new insight in cell proliferation and cell differentiation review. Curr Clin Pharmacol 2008;3(1):38–45.

9. Black KL, Ikezaki K, Santori E, Becker DP, Vinters HV. Specific high-affinity binding of peripheral benzodiazepine receptor ligands to brain tumors in rat and man. Cancer 1990;65(1):93–7.

10. Junck L, Olson JM, Ciliax BJ, Koeppe RA, Watkins GL, Jewett DM, et al. PET imaging of human gliomas with ligands for the peripheral benzodiazepine binding site. Ann Neurol 1989;26 (6):752–8.

11. Olson JM, Junck L, Young AB, Penney JB, Mancini WR. Isoquinoline and peripheral-type benzodiazepine binding in gliomas: implications for diagnostic imaging. Cancer Res 1988;48(20):5837–41.

12. Starosta-Rubinstein S, Ciliax BJ, Penney JB, McKeever P, Young AB. Imaging of a glioma using peripheral benzodiazepine receptor ligands. Proc Natl Acad Sci U S A 1987;84(3):891–5.

13. Benavides J, Cornu P, Dennis T, Dubois A, Hauw JJ, MacKenzie ET, et al. Imaging of human brain lesions with an omega 3 site radioligand. Ann Neurol 1988;24(6):708–12.

14. Syapin PJ, Skolnick P. Characterization of benzodiazepine binding sites in cultured cells of neural origin. J Neurochem 1979;32 (3):1047–51.

15. Miettinen H, Kononen J, Haapasalo H, Helén P, Sallinen P, Harjuntausta T, et al. Expression of peripheral-type benzodiazepine receptor and diazepam binding inhibitor in human astrocytomas: relationship to cell proliferation. Cancer Res 1995;55(12):2691–5.

16. Vlodavsky E, Soustiel JF. Immunohistochemical expression of peripheral benzodiazepine receptors in human astrocytomas and its correlation with grade of malignancy, proliferation, apoptosis and survival. J Neurooncol 2007;81(1):1–7.

17. Pappata S, Cornu P, Samson Y, Prenant C, Benavides J, Scatton B, et al. PET study of carbon-11-PK 11195 binding to peripheral type benzodiazepine sites in glioblastoma: a case report. J Nucl Med 1991;32(8):1608–10.

18. Chauveau F, Van Camp N, Dollé F, Kuhnast B, Hinnen F, Damont A, et al. Comparative evaluation of the translocator protein radioligands 11C-DPA-713, 18F-DPA-714, and 11C-PK11195 in a rat model of acute neuroinflammation. J Nucl Med 2009;50(3):468–76.

19. Lodi F, Trespidi S, Di Pierro D, Marengo M, Farsad M, Fanti S, et al. A simple Tracerlab module modification for automated on-column [11C]methylation and [11C]carboxylation. Appl Radiat Isot 2007;65(6):691–5.

20. James ML, Fulton RR, Vercoullie J, Henderson DJ, Garreau L, Chalon S, et al. DPA-714, a new translocator protein-specific ligand: synthesis, radiofluorination, and pharmacologic characterization. J Nucl Med 2008;49(5):814–22.

21. Kuhnast B, Damont A, Hinnen F, Catarina T, Demphel S, Le Helleix S, et al. [(18)F]DPA-714, [(18)F]PBR111 and [(18)F] FEDAA1106–selective radioligands for imaging TSPO 18 kDa with PET: automated radiosynthesis on a TRACERLAb FX-FN synthesizer and quality controls. Appl Radiat Isot 2011 [Epub ahead of print].

22. Damont A, Hinnen F, Kuhnast B, Schöllhorn-Peyronneau MA, James M, Luus C, et al. Radiosynthesis of [18F]DPA-714, a selective radioligand for imaging the translocator protein (18 kDa) with PET. J Labelled Comp Radiopharm 2008;51(7–8):286–92.

23. Van Camp N, Boisgard R, Kuhnast B, Thézé B, Viel T, Grégoire MC, et al. In vivo imaging of neuroinflammation: a comparative study between [(18)F]PBR111, [(11)C]CLINME and [(11)C] PK11195 in an acute rodent model. Eur J Nucl Med Mol Imaging 2010;37(5):962–72.

24. Čížek J, Herholz K, Vollmar S, Schrader R, Klein J, Heiss WD. Fast and robust registration of PET and MR images of human brain. Neuroimage 2004;22(1):434–42.

25. Groom GN, Junck L, Foster NL, Frey KA, Kuhl DE. PET of peripheral benzodiazepine binding sites in the microgliosis of Alzheimer's disease. J Nucl Med 1995;36(12):2207–10.

26. Kropholler MA, Boellaard R, van Berckel BN, Schuitemaker A, Kloet RW, Lubberink MJ, et al. Evaluation of reference regions for (R)-[(11)C]PK11195 studies in Alzheimer's disease and mild cognitive impairment. J Cereb Blood Flow Metab 2007; 27(12):1965–74.

27. Versijpt JJ, Dumont F, Van Laere KJ, Decoo D, Santens P, Audenaert K, et al. Assessment of neuroinflammation and microglial activation in Alzheimer's disease with radiolabelled PK11195 and single photon emission computed tomography. A pilot study. Eur Neurol 2003;50(1):39–47.

28. Lammertsma AA, Hume SP. Simplified reference tissue model for PET receptor studies. Neuroimage 1996;4(3 Pt 1):153–8.

29. Innis RB, Cunningham VJ, Delforge J, Fujita M, Gjedde A, Gunn RN, et al. Consensus nomenclature for in vivo imaging of reversibly binding radioligands. J Cereb Blood Flow Metab 2007;27 (9):1533–9.

30. Boutin H, Chauveau F, Thominiaux C, Grégoire MC, James ML, Trebossen R, et al. 11C-DPA-713: a novel peripheral benzodiazepine receptor PET ligand for in vivo imaging of neuroinflammation. J Nucl Med 2007;48(4):573–81.

31. Ji B, Maeda J, Sawada M, Ono M, Okauchi T, Inaji M, et al. Imaging of peripheral benzodiazepine receptor expression as biomarkers of detrimental versus beneficial glial responses in mouse models of Alzheimer's and other CNS pathologies. J Neurosci 2008;28(47):12255–67.

32. Martín A, Boisgard R, Thézé B, Van Camp N, Kuhnast B, Damont A, et al. Evaluation of the PBR/TSPO radioligand [(18)F]DPA-714 in a rat model of focal cerebral ischemia. J Cereb Blood Flow Metab 2010;30(1)230–41.

33. Buck JR, McKinley ET, Hight MR, Fu A, Tang D, Smith RA, et al. Quantitative, preclinical PET of translocator protein expression in glioma using 18F-N-fluoroacetyl-N-(2,5-dimethoxybenzyl)-2-phenoxyaniline. J Nucl Med 2011;52(1):107–14.

34. Levin E, Premkumar A, Veenman L, Kugler W, Leschiner S, Spanier I, et al. The peripheral-type benzodiazepine receptor and tumorigenicity: isoquinoline binding protein (IBP) antisense knockdown in the C6 glioma cell line. Biochemistry 2005;44 (29):9924–35.

35. Stojiljkovic M, Piperski V, Dacevic M, Rakic L, Ruzdijic S, Kanazir S. Characterization of 9L glioma model of the Wistar rat. J Neurooncol 2003;63(1):1–7.

36. Lorusso G, Rüegg C. The tumor microenvironment and its contribution to tumor evolution toward metastasis. Histochem Cell Biol 2008;130(6):1091–103.

37. Badie B, Schartner JM. Flow cytometric characterization of tumor-associated macrophages in experimental gliomas. Neurosurgery 2000;46(4):957–61. discussion 961–2.

38. Parney IF, Waldron JS, Parsa AT. Flow cytometry and in vitro analysis of human glioma-associated macrophages. Laboratory investigation. J Neurosurg 2009;110(3):572–82.

39. Charles NA, Holland EC, Gilbertson R, Glass R, Kettenmann H. The brain tumor microenvironment. Glia 2011;59(8):1169–80.

40. Jacobs AH, Kracht LW, Gossmann A, Rüger MA, Thomas AV, Thiel A, et al. Imaging in neurooncology. NeuroRx 2005;2 (2):333–47.

41. Dhermain FG, Hau P, Lanfermann H, Jacobs AH, van den Bent MJ. Advanced MRI and PET imaging for assessment of treatment response in patients with gliomas. Lancet Neurol 2010;9(9):906–20.

42. Kläsner BD, Krause BJ, Beer AJ, Drzezga A. PET imaging of gliomas using novel tracers: a sleeping beauty waiting to be kissed. Expert Rev Anticancer Ther 2010;10(5):609–13.

43. Venneti S, Lopresti BJ, Wang G, Slagel SL, Mason NS, Mathis CA, et al. A comparison of the high-affinity peripheral benzodiazepine receptor ligands DAA1106 and (R)-PK11195 in rat models of neuro-inflammation: implications for PET imaging of microglial activation. J Neurochem 2007;102(6):   2118–31.

44. Fujimura Y, Zoghbi SS, Simèon FG, Taku A, Pike VW, Innis RB, et al. Quantification of translocator protein (18 kDa) in the human brain with PET and a novel radioligand, (18)F-PBR06. J Nucl Med 2009;50(7):1047–53.

45. Imaizumi M, Briard E, Zoghbi SS, Gourley JP, Hong J, Fujimura Y, et al. Brain and whole-body imaging in nonhuman primates of [11C]PBR28, a promising PET radioligand for peripheral benzo-diazepine receptors. Neuroimage 2008;39(3):1289–98.

46. Barth RF, Kaur B. Rat brain tumor models in experimental neuro-oncology: the C6, 9L, T9, RG2, F98, BT4C, RT-2 and CNS-1 gliomas. J Neurooncol 2009;94(3):299–312.

47. Orringer DA, Chen T, Huang DL, Armstead WM, Hoff BA, Koo YE, et al. The brain tumor window model: a combined cranial window and implanted glioma model for evaluating intraoperative contrast agents. Neurosurgery 2010;66(4):736–43.

48. Herz RCG, Jonker M, Verheul HB, Hillen B, Versteeg DHG, de Wildt DJ. Middle cerebral artery occlusion in Wistar and Fischer-344 rats: functional and morphological assessment of the model. J Cereb Blood Flow Metab 1996;16(2):296–302.

49. Fujita M, Imaizumi M, Zoghbi SS, Fujimura Y, Farris AG, Suhara T, et al. Kinetic analysis in healthy humans of a novel positron emission tomography radioligand to image the peripheral benzo-diazepine receptor, a potential biomarker for inflammation. Neuro-image 2008;40(1):43–52.

50. Owen DR, Gunn RN, Rabiner EA, Bennacef I, Fujita M, Kreisl WC, et al. Mixed-affinity binding in humans with 18-kDa trans-locator protein ligands. J Nucl Med 2011;52(1):24–32.

51. Owen DR, Howell OW, Tang SP, Wells LA, Bennacef I, Bergstrom M, et al. Two binding sites for [3H]PBR28 in human brain: implications for TSPO PET imaging of neuroinflammation. J Cereb Blood Flow Metab 2010;30(9):1608–18.

52. Owen DR, Yeo AJ, Gunn RN, Song K, Wadsworth G, Lewis A, et al. An 18-kDa translocator protein (TSPO) polymorphism explains differences in binding affinity of the PET radioligand PBR28. J Cereb Blood Flow Metab 2011 [Epub ahead of print].

53. Le DM, Besson A, Fogg DK, Choi KS, Waisman DM, Goodyer CG, et al. Exploitation of astrocytes by glioma cells to facilitate invasiveness: a mechanism involving matrix metalloproteinase-2 and the urokinase-type plasminogen activator-plasmin cascade. J Neurosci 2003;23(10):4034–43.